Available online at www.sciencedirect.com
ScienceDirect
C. R. Mecanique 335 (2007) 168–174
COMPTES RENDUS MECANIQUE
http://france.elsevier.com/direct/CRAS2B/

Refined experimental methodology for assessing the heat dissipated in cyclically loaded materials at low stress levels

François Maquin *, Fabrice Pierron

Laboratoire de mécanique et procédés de fabrication (LMPF), École nationale supérieure d'arts et métiers, rue St Dominique, BP 508, 51006 Châlons-en-Champagne cedex, France

Received 21 August 2006; accepted after revision 6 February 2007

Available online 2 April 2007

Presented by André Zaoui

Abstract

The present study is aimed at studying the heat generated in steel specimens cyclically tested at stresses lower than their macroscopic elastic limit, in the objective of detecting the onset of microplasticity. First, the data processing procedure is presented to calculate heat sources and thermal energy levels from temperature maps. Then, a sensitivity study is performed to establish the smallest energy value that can be detected above noise. Finally, results are presented for a cold rolled low carbon steel material. It is shown that two main mechanisms of dissipation are present, the first one corresponding to viscoelastic effects and the second one associated to microplasticity. ***To cite this article: F. Maquin, F. Pierron, C. R. Mecanique 335 (2007).***

Résumé

Méthodologie fine de détermination de la chaleur dissipée dans un matériau chargé cycliquement à faible contrainte. Cette étude traite de la mesure de l'énergie dissipée sous forme de chaleur au sein d'éprouvettes d'un acier bas carbone laminé à froid, testées cycliquement à des niveaux de contrainte inférieurs à sa limite d'élasticité macroscopique, dans l'objectif de déterminer sa limite de microplasticité. Dans un premier temps, la procédure de traitement des données est présentée, permettant de calculer les sources de chaleur et l'énergie dissipée à partir des mesures de température. Ensuite, une étude du bruit de mesure est présentée. Finalement, on met en évidence deux phénomènes dissipatifs : le premier correspondant à de la viscoélasticité et le second associé à la microplasticité. ***Pour citer cet article : F. Maquin, F. Pierron, C. R. Mecanique 335 (2007).***

Keywords: Heat transfer; Heat dissipation; Cyclic loading; Thermomechanical behaviour

Mots-clés : Transferts thermiques ; Dissipation de chaleur ; Essais cycliques ; Thermomécanique

* Corresponding author.
E-mail addresses: francois.maquin@chalons.ensam.fr (F. Maquin), fabrice.pierron@chalons.ensam.fr (F. Pierron).

1631-0721/$ – see front matter
doi:10.1016/j.crme.2007.02.004

1. Introduction

A metallic material cyclically loaded at stress levels corresponding to high cycle fatigue (i.e., well below the macroscopic elastic limit) heats up. The heat sources responsible for this behaviour are of two kinds. The first are caused by the thermoelastic coupling effect. They are in phase with the load and proportional to the elastic deformation (and therefore, cyclic) and are the basis of the thermoelastic strain measurement techniques. The second ones, of much lower intensities and of irreversible nature, are associated with dissipation mechanisms within the material at the microscale during deformation. By observing the increase of temperature over a few thousands of cycles, many authors [1–4] notice a change of the heating rate for a stress level close to the fatigue limit. This approach is very promising in the framework of the reduction of fatigue testing time; however, it proved to be rather unreliable, working only for certain materials, and should, to the opinion of the present authors, rely on a more physical base to be able to relate this change of thermomechanical regime to the microstructural changes taking place in the tested material. The present study deals with the observation of the heat sources during the very first fatigue cycles. The objective is to relate the measurement of the intrinsic dissipation to the activation of different micro-mechanisms: viscoelastic effects related, among others, to the reversible movement of anchored dislocations at low stress levels and microplasticity effects corresponding to the irreversible movements of dislocations (Frank-Read source, for instance) [5]. After recalling the main hypotheses and the equations involved in the calculation of the heat sources and energy, the sensitivity of energy detection is evaluated and experimental results are presented for a cold rolled low carbon steel material.

2. Experimental procedure

As rightly stated by Chrysochoos et al. [6], the variation of temperature is not an intrinsic manifestation of the material behaviour since it is affected by the conditions of thermal exchanges by conduction, convection and radiation between the observed part of the specimen and its environment. It is therefore necessary to resort to the calculation of the heat sources to obtain intrinsic parameters to be related to the material behaviour. The procedure used in this paper is strongly inspired from the approach developed by Chrysochoos et al. [6], except that since the energy levels that will be recorded are extremely small, thorough attention has been paid to suppress all sources of discrepancies.

Fig. 1 shows the experimental arrangement. All tests have been performed on plane specimens with a rectangular active gauge section (thickness $e = 1.5$ mm, width $l = 20$ mm and gauge length $lu = 30$ mm), see Fig. 1. Careful protection of the environment around the test specimen has been provided to avoid external radiative reflections onto the specimen. It can also be seen on Fig. 1 that the bottom grip, connected to the actuator, has had to be cooled down by circulating water in order to reduce its radiative reflection onto the specimen. The material used in this study is a very low carbon steel sheet. Its elastic limit at 0.2% strain is about 180 MPa. The specimens are tested cyclically using a hydraulic actuator at two stress ratios $R_\sigma = \frac{\sigma_{\mathrm{MIN}}}{\sigma_{\mathrm{MAX}}} = 0.1$ and -1, and a frequency of 15 Hz, at stress levels lower than the macroscopic elastic limit. The choice of the frequency was made such that it is high enough so that the dissipation leads to temperatures high enough to be detected and so that the thermoelastic effect can easily be extracted (see below). However, there is a limitation coming from our servohydraulic machine, so 15 Hz was the highest frequency

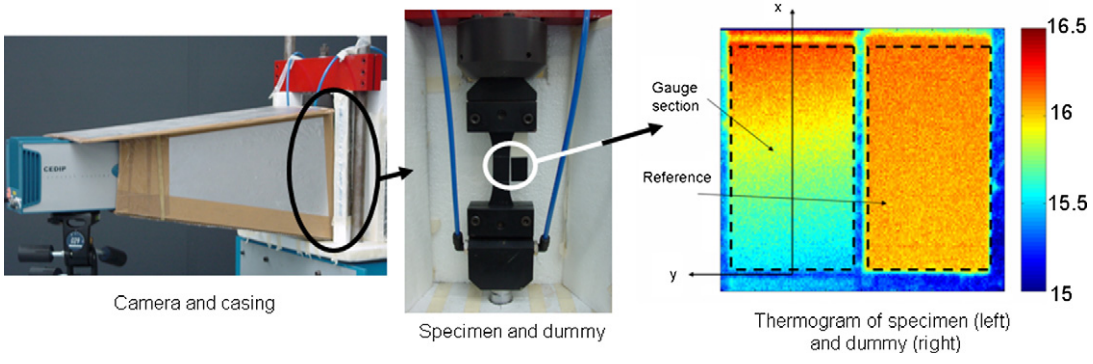

Fig. 1. Relative positions of the tested and reference specimens.

that was achievable. It must be noted, however, that there is also a limit coming from the sampling rate of the camera itself if higher frequencies are to be used. A dummy specimen (see Fig. 1) is positioned next to the tested one in order to monitor the changes of environmental conditions. The temperature fields are captured using a 350 Hz sampling infrared camera (CEDIP Jade III) with a resolution of 160×120 pixels. As a consequence of the experimental set up, both specimen and reference are covered by about 5000 pixels each. Both test specimen and dummy are painted in black to enhance their emissivity. The storing capacity of the camera system limits the acquisition to 3500 successive images, which corresponds roughly to 10 seconds of recording: 5 seconds before starting the actuator and 5 seconds of test. In the following, the heat sources are computed over the first 3 seconds after the start of the test, which correspond to 45 load cycles. The heat sources are supposed to be uniformly distributed throughout the specimen and the temperature is considered constant throughout the thickness of the specimen, transforming the 3D problem into a 2D one. Neglecting the heat exchanges over the through-thickness sides of the specimen, the heat fluxes can be sorted in three: in-plane conduction at the end of the specimen (near the grips), convection and radiation over the front and back faces of the specimen. Denoting w_{ch} the volume density of the thermo-mechanical heat sources activated during the deformation of the material, $T_e(t)$ the temperature of the environment and $T(x, y, t)$ the measured surface temperature field, the thermal energy balance per unit volume at any point (x, y) of the surface of the gauge section can be written as [7]:

$$\rho C \frac{\partial T(x,y,t)}{\partial t} - k\Delta T(x,y,t) + \frac{2\sigma_e \varepsilon_m T^4(x,y,t)}{e} + \frac{2h}{e}\big(T(x,y,t) - T_e(t)\big) = w_{\mathrm{ch}} + r_{\mathrm{spec}} \tag{1}$$

where C is the specific heat and k the thermal conductivity of the material, σ_e the Stefan–Boltzmann constant, ε_m the emissivity, h the convection heat exchange coefficient and r_{spec} the external sources acting on the specimen (for instance, the radiative reflection from the environment). In this equation, the left-hand side terms represent, respectively, the heat rate of a unit volume element, the conduction heat flux and the radiative and convective heat fluxes. At $t = 0$, just before the start of the test, the heat sources are still zero. Therefore, Eq. (1) can be written as:

$$\rho C \frac{\partial T}{\partial t}_{t=0} - k\Delta T_0 + \frac{2\sigma_e \varepsilon_m T_0^4}{e} + \frac{2h}{e}(T_0 - T_{0e}) = r_{0\mathrm{spec}} \tag{2}$$

where the subscript zero denotes the value of the corresponding parameter at $t = 0$. Subtracting from Eq. (1) and denoting $\theta_{\mathrm{spec}}(x, y, t) = T(x, y, t) - T_0(x, y)$ (subtraction of the last image just before the start of the actuator)), it results in:

$$\rho C\left[\frac{\partial \theta_{\mathrm{spec}}}{\partial t} - \frac{\partial \theta_{\mathrm{spec}}}{\partial t}_{t=0}\right] - k\Delta\theta_{\mathrm{spec}} + \frac{2\sigma_e \varepsilon_m}{e}\big(T^4(x,y,t) - T_0^4\big) + \frac{2h}{e}\theta_{\mathrm{spec}} - \frac{2h}{e}\theta_e = w_{\mathrm{ch}} + r_{\mathrm{spec}} - r_{0\mathrm{spec}} \tag{3}$$

where $\theta_e = T_e(t) - T_{0e}$. By linearizing the radiative term in the above equation [7], Eq. (3) becomes:

$$\rho C\left[\frac{\partial \theta_{\mathrm{spec}}}{\partial t} - \frac{\partial \theta_{\mathrm{spec}}}{\partial t}_{t=0}\right] - k\Delta\theta_{\mathrm{spec}} + \rho C\frac{\theta_{\mathrm{spec}}}{\tau_{\mathrm{th}}} - \frac{2h}{e}\theta_e = w_{\mathrm{ch}} + r_{\mathrm{spec}} - r_{0\mathrm{spec}} \tag{4}$$

where τ_{th} is a time constant. The next step is to integrate Eq. (4) over x and y. The temperature is supposed to be independent of the y coordinate. By denoting $\bar{\bar{T}}(t)$ the x and y spatial average of the temperature and $\bar{\bar{\theta}}(t) = \bar{\bar{T}}(t) - T_0$, Eq. (4) becomes:

$$\rho C\left[\frac{\partial \bar{\bar{\theta}}_{\mathrm{spec}}}{\partial t} - \frac{\partial \bar{\bar{\theta}}_{\mathrm{spec}}}{\partial t}_{t=0}\right] - \frac{k}{lu}\int_{-lu/2}^{lu/2} \frac{\partial \bar{\theta}_{\mathrm{spec}}(x,t)}{\partial x_2}\,\mathrm{d}x + \rho C\frac{\bar{\bar{\theta}}_{\mathrm{spec}}}{\tau_{\mathrm{th}}} - \frac{2h}{e}\bar{\bar{\theta}}_e = \bar{\bar{w}}_{\mathrm{ch}} + \bar{\bar{r}}_{\mathrm{spec}} - \bar{\bar{r}}_{0\mathrm{spec}} \tag{5}$$

where $\bar{\bar{w}}_{\mathrm{ch}}$ is the spatial average of the heat sources. Finally, it is necessary to use the dummy to eliminate the variations of the temperature of the environment. By applying (Eq. (5)) to the dummy:

$$\rho C\left[\frac{\partial \bar{\bar{\theta}}_{\mathrm{ref}}}{\partial t} - \frac{\partial \bar{\bar{\theta}}_{\mathrm{ref}}}{\partial t}_{t=0}\right] + \rho C\frac{\bar{\bar{\theta}}_{\mathrm{ref}}}{\tau_{\mathrm{th}}} - \frac{2h}{e}\bar{\bar{\theta}}_{e\,\mathrm{ref}} = \bar{\bar{r}}_{\mathrm{ref}} - \bar{\bar{r}}_{0\mathrm{ref}} \tag{6}$$

By denoting $\theta = \bar{\bar{\theta}}_{\mathrm{spec}} - \bar{\bar{\theta}}_{\mathrm{ref}}$, and supposing that $\bar{\bar{\theta}}_e = \bar{\bar{\theta}}_{e\,\mathrm{ref}}$ and subtracting Eq. (6) from Eq. (5), the final equation is:

$$\rho C\left[\frac{\partial \bar{\bar{\theta}}}{\partial t} - \frac{\partial \bar{\bar{\theta}}}{\partial t}_{t=0}\right] - \frac{k}{lu}\int_{-lu/2}^{lu/2} \frac{\partial \bar{\theta}_{\mathrm{spec}}(x,t)}{\partial x_2}\,\mathrm{d}x + \rho C\frac{\bar{\bar{\theta}}}{\tau_{\mathrm{th}}} = \bar{\bar{w}}_{\mathrm{ch}} \tag{7}$$

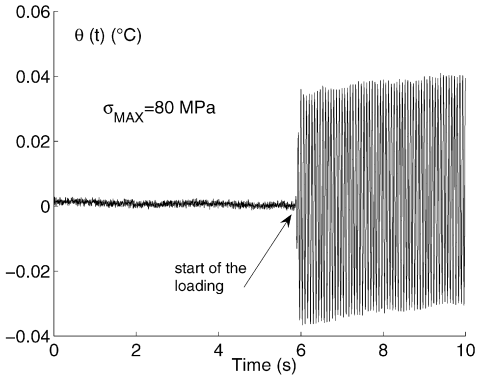

Fig. 2. Raw temperature signal.

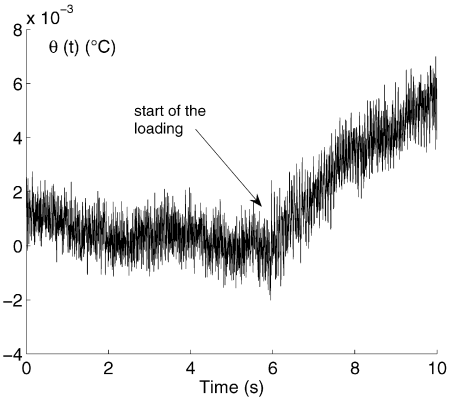

Fig. 3. Temperature signal without the thermoelastic term.

where it was also supposed that the effect of the radiative reflection of the environment was the same on the specimen and the dummy, therefore, $\bar{\bar{r}}_{\text{spec}} - \bar{\bar{r}}_{0\text{spec}} = \bar{\bar{r}}_{\text{ref}} - \bar{\bar{r}}_{0\text{ref}}$. This is the reason why the bottom grip had to be cooled, because the mounting of the dummy and the specimen is not symmetrical with respect to the grip, hence a relative variation of radiative reflection that had to be reduced. In the present case, the heat sources term is composed of two main contributions: the thermoelastic coupling term that will be evidenced as a harmonic temperature variation at the excitation frequency and the intrinsic dissipation term which will tend to heat up the specimen. Since the focus is placed on this second term in the present study, the first step in the processing of the temperature field is to filter out the thermoelastic term. This has been performed in the same spirit as in [6], only here, the temperature variations caused by the thermoelastic effect, expressed as

$$\bar{\bar{\theta}}_{\text{th}\,e}(t) = -\alpha\big(\sigma(t) - \sigma_m\big)\frac{T_0}{\rho C} \tag{8}$$

have been subtracted directly from the signal (α is the coefficient of thermal expansion of the material and σ_m the mean stress of the loading cycle). The stress signal $\sigma(t)$ is calculated from that given by the load cell, the thermophysical constants have been retrieved from the literature and T_0 is the average temperature from the active area of the tested specimen. It must be noted that when doing so, usually, a slight thermoelastic residual remains (typically, 1 to 2% of the initial amplitude) because of the uncertainties on the different quantities. A small multiplicative correction factor is then applied to zero it completely. As an example, Figs. 2 and 3 show the signal before and after the removal of the thermoelastic term. It can be seen on these figures that the temperature changes caused by the thermoelastic effect are much larger than the ones caused by the intrinsic dissipation in the present case. After this operation, two problems remain to calculate the dissipative heat sources: temporal differentiation for the heat rate term and double spatial differentiation for the Laplacian term. The first one is achieved by a local polynomial fitting of degree 4 over a sliding window of ± 250 points. This is a good compromise to filter out the remaining noise but still be able to evaluate the evolution of the heat sources as a function of time during these 3 seconds. A systematic study was performed to reach this conclusion [8]. $\frac{\partial \bar{\bar{\theta}}}{\partial t}_{t=0}$ is simply computed as the slope of the line fitting the data before the start of the actuator. The Laplacian is evaluated by fitting a second order polynomial in x to $\bar{\theta}_{\text{spec}}(x,t)$. This approach is very similar to that in [6]. It must be noted however that due to the very short testing time, the process is nearly adiabatic here and the Laplacian and radiative/convective terms are very small, with experimental measurement of τ_{th} at the beginning of each test using a cooling down test. Finally, from the heat sources, it is possible to calculate the energy dissipated during these 45 loading cycles by time integration. This will provide an additional smoothing of the data. It is performed by simple rectangle integration.

3. Results

Since the amount of energy released during these few cycles will be extremely small, it is of primary importance to evaluate the detection threshold of the experiment. To do so, the procedure above is applied onto a series of data

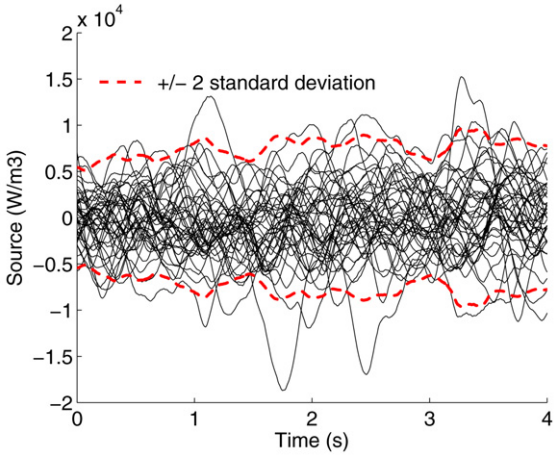

Fig. 4. Heat sources from noise data.

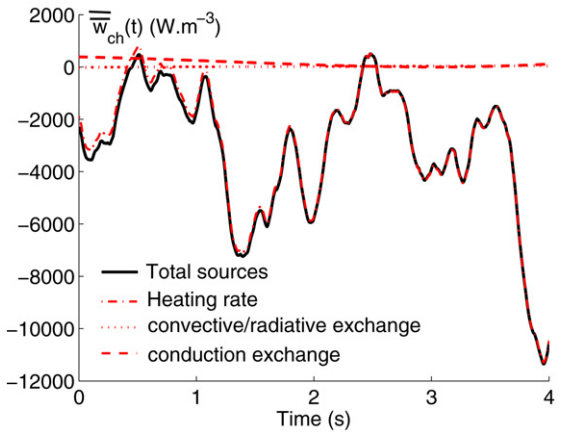

Fig. 5. Decomposition of a typical heat source signal: relative values of heating rate and conductive and radiative/convective exchanges.

where the test specimen is at rest and values for heat sources and energy are recorded. Fig. 4 shows a series of results coming from 41 tests. The dotted line is a representation of the noise at plus or minus twice the standard deviation. These curves will be used on subsequent plots to indicate the detection threshold. By integrating these curves, a detection threshold of 6.5×10^3 J m^{-3} is obtained for the energy after 3 seconds. Dividing this energy by ρC, it can be expressed in °C as the amount of energy required to increase the specimen temperature this much. Since for this material, $\rho = 7800$ kg m^{-3} and $C = 460$ J kg^{-1} °C^{-1}, this energy corresponds to 1.8 mK. The reason why this is so small is that not only the performances of the CEDIP Jade III camera are excellent but also the extensive smoothing coming from the spatial averaging of the temperature information (the double bars in Eq. (7)), plus the averaging coming from the time integration to obtain the energy. This means that the present procedure provides an extremely sensitive tool to monitor heat releases in material testing. It should also be noted that among the three terms of the left hand-side of Eq. (7), the first term (heating rate) is largely predominant over the two others (which represent the heat losses, either by conduction or convection/radiation), as can be seen on Fig. 5.

The tests are carried out at maximum stress levels σ_{MAX} ranging from 40 to 180 MPa for $R_\sigma = 0.1$ and from 20 to 100 MPa for $R_\sigma = -1$, buckling appearing beyond in this case. A virgin specimen is used for each level of loading. During the tests with purely alternate loading (Fig. 6), the sources are constant in time after a short time of regular growth corresponding to time necessary to the regulation of the jack to reach its set point. On the other hand, in the case of the positive loading ratio (Fig. 7), for the highest levels of stress, the sources increase sharply during the first second and then stabilize. This transitory behaviour is certainly due to a phenomenon of micro-plastic cyclic adaptation, followed by a viscoelastic behaviour caused by internal friction. It is interesting to note that by comparing the levels of the sources for two tests at the same strain rate (Fig. 8) but with different maximum stresses, one observes that they converge towards the same stabilized level of thermal sources. By representing the values of the energy dissipated during the two first seconds of the test as a function of the maximum strain rate (Fig. 9), one observes very close values between the two stress ratios up to about 0.03 s^{-1}, that is to say 140 MPa for $R_\sigma = 0.1$, with slightly higher values in this case but with differences of the order of the detection threshold. Beyond, the dissipated energy is more important for $R_\sigma = 0.1$ than for $R_\sigma = -1$ for the same strain rate, clearly indicating a change of material behaviour. For a traditional linear viscoelastic behaviour, the theoretical intrinsic dissipation is equal to the product of the anelastic stress by the strain rate, the first being itself proportional to the strain rate. Therefore, the dissipation will be a quadratic function of the strain rate, which is consistent with the data for $R_\sigma = -1$ for which the maximum stress reached was only 100 MPa. However, when microplasticity occurs, the intrinsic dissipation will depart from this quadratic evolution, which is what happens at $R_\sigma = 0.1$ after 140 MPa. Obviously, to fully confirm this conclusion, tests at $R_\sigma = -1$ up to 180 MPa should be performed but this is more difficult because of buckling effects. The gauge section has to be drastically reduced, which causes other problems. Another way of checking these results would be change the loading frequency.

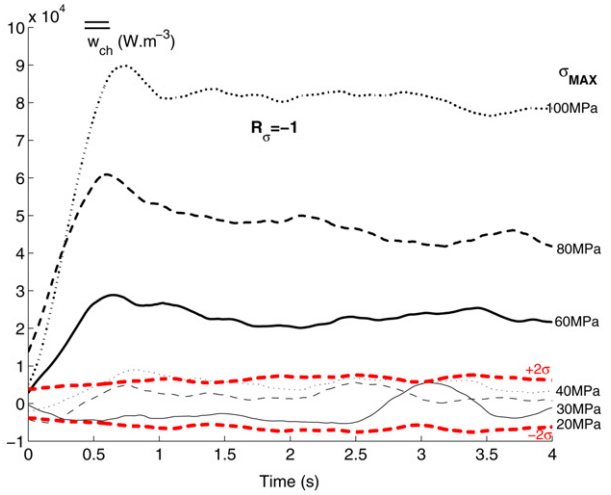

Fig. 6. Temporal evolution of the heat sources over 4 seconds as a function of the maximal stress level, $R_\sigma = -1$.

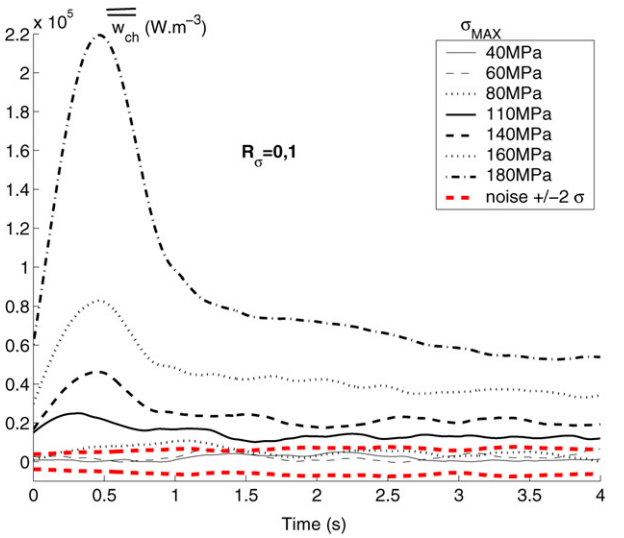

Fig. 7. Temporal evolution of the heat sources over 4 seconds as a function of the maximal stress level, $R_\sigma = 0.1$.

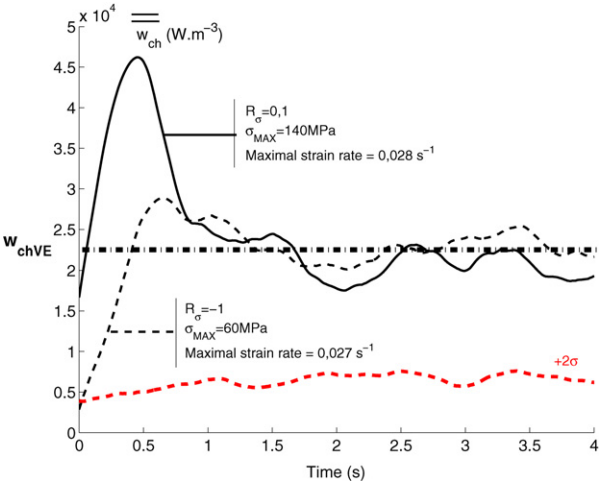

Fig. 8. Comparison of the temporal evolution of the heat sources for two tests: one at $R_\sigma = 0.1$ and one at $R_\sigma = -1$, with different stress levels but similar strain rates.

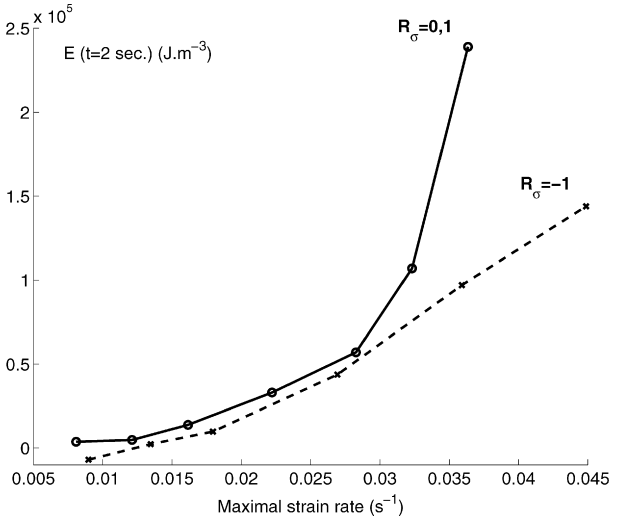

Fig. 9. Energy dissipated after 2 seconds, for both stress ratios, as a function of the strain rate.

4. Conclusion

The present results are obviously incomplete but the paper clearly shows that it is possible to measure with confidence very small quantities of heat by using an appropriate and original procedure relying on spatial averaging and accounting of the non stability of the thermal state of the sample. The thorough evaluation of the detection threshold on the heat sources guarantees the significance of the results. Concerning the test results, it is shown that by comparing results at different strain rates, it is possible to detect significant changes in the heat dissipation regime that are certainly related to the onset of microplasticity. Future work involves complementary testing at other frequencies and stress ratios to confirm the present findings as well as tests using strain measurements at the microscale [9] to confirm the onset of microplasticity.

References

[1] R. Harry, F. Joubert, A. Gooma, Measuring the actual endurance limit of one specimen using a nondestructive method, Journal of Engineering Materials and Technology (ASME) 103 (1) (1981) 71–76.
[2] M.P. Luong, Fatigue limit evaluation of metals using an infrared thermographic technique, Mechanics of Materials 28 (1998) 155–163.
[3] G. La Rosa, A. Risitano, Thermographic methodology for rapid determination of the fatigue limit of materials and mechanical components, International Journal of Fatigue 22 (2000) 65–73.
[4] F. Curà, G. Curti, R. Essana, A new method for the thermographic determination of fatigue limit in steels, International Journal of Fatigue 27 (2005) 453–459.
[5] D. François, A. Pineau, A. Zaoui, Comportement mécanique des matériaux solides, Hermès (1995) 217–218.
[6] T. Boulanger, A. Chrysochoos, C. Mabru, A. Galtier, Calorimetric analysis of dissipative and thermoelastic effects associated with the fatigue behavior of steels, International Journal of Fatigue 26 (3) (2004) 221–229.
[7] H. Louche, A. Chrysochoos, Thermal and dissipative effects accompanying Lüders band propagation, Materials Science and Engineering A 307 (1–2) (2001) 15–22.
[8] F. Maquin, Méthodologie expérimentale d'étude du comportement thermo-mécanique des matériaux sous sollicitations cycliques, PhD thesis, ENSAM, France, 2006.
[9] R. Moulart, R. Rotinat, F. Pierron, G. Lerondel, Optical full-field measurement of strain at a microscopic scale with the grid method, in: Speckle 06, 2006, 13–15 September, Nîmes, France.